A novel, NADH-dependent acrylate reductase in *Vibrio harveyi*

Yulia V. Bertsova, Marina V. Serebryakova, Alexander A. Baykov, and Alexander V. Bogachev*

Belozersky Institute of Physico-Chemical Biology, Lomonosov Moscow State University, Moscow 119234*, Russia.*

Running Title: Acrylate reduction in *V. harveyi*

*For correspondence: bogachev@belozersky.msu.ru

Abstract

Bacteria coping with oxygen deficiency use alternative terminal electron acceptors for NADH regeneration, particularly fumarate. Fumarate is reduced by the *FAD_binding_2* domain of cytoplasmic fumarate reductase in many bacteria. The variability of the primary structure of this domain in homologous proteins suggests the existence of reducing activities with different specificities. Here we produced and characterized one such protein, *Vibrio harveyi* ARD, and found it to be a specific NADH:acrylate oxidoreductase. This previously unknown enzyme contains covalently bound FMN and non-covalently bound FAD and FMN in a ratio of 1:1:1. The covalently bound FMN is absolutely required for activity and is attached by the specific flavin transferase, ApbE, to a threonine residue in the auxiliary *FMN_bind* domain. RT-qPCR and activity measurements indicated dramatic stimulation of ARD biosynthesis by acrylate in the *V. harveyi* cells grown aerobically. In contrast, the *ard* gene expression in the cells grown anaerobically was high without acrylate and increased only twofold in its presence. These findings suggest that the principal role of ARD in *Vibrio* is energy-saving detoxification of acrylate coming from the environment.

Importance

The benefits of the massive genomic information accumulated in recent years for biological sciences have been limited by the lack of data on the function of most gene products. Approximately half of the known prokaryotic genes are annotated as “proteins with unknown functions,” and many other genes are annotated incorrectly. Thus, the functional and structural characterization of the products of such genes, including identification of all existing enzymatic activities, is a pressing issue in modern biochemistry. In this work, we have shown that the *ard* gene product of *V. harveyi* (GenBank ID: AIV07243) exhibits a yet undescribed NADH:acrylate oxidoreductase activity. This activity may allow acrylate detoxification and its use as a terminal electron acceptor in anaerobic or substrate in aerobic respiration of marine and other bacteria.

36 **INTRODUCTION**

37 Many microbes are capable of anaerobic respiration by using various organic and inorganic
38 compounds instead of oxygen as terminal electron acceptors in the respiratory electron transport
39 chain. Fumarate is a typical organic terminal acceptor commonly reduced by membrane-bound
40 quinol:fumarate oxidoreductase complex, similar to the Complex II of the respiratory chain (1).
41 In some microbes, fumarate is reduced by a soluble monomeric enzyme using cytochrome *c*,
42 NADH, or flavin as the source of reducing equivalents during anaerobic respiration (2–6). In
43 both types of fumarate-reducing enzymes, fumarate is bound and converted by a *FAD_binding_2*
44 domain (Pfam ID: PF00890).

45 Soluble cytoplasmic NADH:fumarate oxidoreductase from the facultative anaerobic
46 bacterium *Klebsiella pneumoniae* (FRD) is formed by three domains: *OYE-like*, *FMN_bind,* and
47 *FAD_binding_2* (5, 7) (Fig. 1A). The *FAD_binding_2* domain contains a fumarate-binding site
48 and a non-covalently bound FAD molecule. The *OYE-like* domain (PF00724) contains a non-
49 covalently bound FMN molecule and is responsible for NADH oxidation. The domain
50 *FMN_bind* (PF04205) carries out electron transfer between the two other domains and contains
51 an FMN residue covalently linked through a phosphoester bond (5). The catalytic mechanism of
52 fumarate reduction has been described for the soluble fumarate reductase (flavocytochrome *c*,
53 Fcc_3) of the bacterial genus *Shewanella* (2, 3). The reaction involves hydride ion transfer from a
54 nearby (3.2 Å) FAD molecule to the fumarate C2 atom, accompanied by proton transfer to the
55 C3 atom via a proton-conducting channel, and yields succinate (3). X-ray structural studies of
56 *Shewanella frigidimarina* Fcc_3 have pinpointed three groups of functionally important amino
57 acid residues: those binding the C4 carboxylate (Arg402, His504, and Arg544; Motif I) and C1
58 carboxylate (His365 and Thr377; Motif II) and those forming the proton conductance channel
59 (Glu378, Arg381, and Arg402; Motif III) (Fig. 1B) (3). All these residues are conserved in *K.*
60 *pneumoniae* fumarate reductase (Table 1).

61 Genes encoding proteins with the *FAD_binding_2* domain in their structures are ubiquitous
62 among bacterial genomes. However, some of these proteins are unlikely to be fumarate
63 reductases because the residues responsible for C1 carboxylate binding and proton transfer are
64 not conserved in this domain. Three of such proteins have been characterized and indeed found
65 to exhibit different substrate specificities—they preferentially reduce methacrylate (8, 9) or
66 urocanate (10, 11) with cytochrome *c* as the second substrate (Table 1). Motifs I and III are
67 highly conserved in all these enzymes, whereas Motif II is only partially conserved. These
68 findings suggest that substrate specificity within this group of fumarate analogs is determined by
69 Motif II residues, consistent with the X-ray crystallographic data for *S. frigidimarina* fumarate
70 reductase (3).

71 Here we tested this prediction with the *FAD_binding_2* domain-containing protein ARD
72 (GenBank ID: AIV07243) found in the *Vibrio harveyi* genome. ARD and similar proteins of the
73 genus *Vibrio* resemble *K. pneumoniae* NADH:fumarate oxidoreductase by domain composition
74 but largely differ from this enzyme and all other reductases listed in Table 1 not only in Motif II
75 but also in Motif III (Table 1). Specifically, the histidine residue of Motif II is replaced by
76 methionine, and only one arginine residue (affiliated with both Motifs I and III) is conserved in
77 Motif III in comparison with the fumarate reductase sequences. Consistent with these structural
78 differences, the results below identified ARD as the reductase enzyme with yet unknown
79 substrate specificity.
80
81 **RESULTS**
82 **1. Isolation of *V. harveyi* ARD and identification of bound flavins**
83 The *ard* gene was amplified from *V. harveyi* genomic DNA and cloned into the pBAD-
84 TOPO vector that adds a 6×His tag to protein C-terminus. The ARD *FMN_bind* domain contains
85 a D_{449}VISGA**T**$_{455}$ signature motif for the attachment of FMN via a covalent phosphoester bond
86 to the threonine residue (12). To verify this prediction, we expressed the *ard* gene in *E. coli* in
87 the absence and presence of the plasmid pΔhis3 (13), which harbors the gene for the cytoplasmic
88 form of *V. cholerae* flavin transferase ApbE with broad substrate specificity (12). Metal affinity
89 chromatography of the cytoplasmic fractions of the ApbE-lacking and ApbE-producing cells
90 yielded bright yellow 95-kDa proteins (Fig. 2B) in both cases (the calculated mass of 6×His
91 tagged ARD is 112 kDa). A MALDI-MS analysis of the trypsin-digested protein bands revealed
92 the full-length *ard* gene product in the ARD preparations isolated from ApbE-containing and
93 ApbE-lacking cells (sequence coverage of 86 and 92%, respectively). Furthermore, both the N-
94 and C-terminal peptides were present in the mass spectrum, and their amino acid sequences were
95 confirmed by MS/MS analysis (see Supplementary Material). The difference between the
96 measured and theoretical masses is not thus caused by ARD fragmentation and likely results
97 from its anomalous (increased) electrophoretic mobility.
98 The optical spectra of the isolated proteins (Fig. 2A) demonstrated absorbance maxima at
99 ~380 and ~450 nm, characteristic of flavin prosthetic groups. The absorbances were lower with
100 ARD isolated from ApbE-lacking cells. Moreover, this protein did not fluoresce after SDS-
101 PAGE when illuminated at 473 nm, unlike the protein isolated from ApbE-producing cells (Fig.
102 2B). These observations indicated covalently and non-covalently bound flavin groups in
103 authentic ARD, the latter group(s) being attached by the flavin transferase ApbE.
104 To identify the non-covalently bound flavins, the flavinylated ARD was denatured and
105 separated from the solution by ultrafiltration through a 50-kDa cut-off filter. The filtrate

106 contained two-thirds of the initial flavin content, as determined spectrophotometrically. HPLC
107 analysis of the filtrate identified FAD and FMN in equal amounts (Fig. 2C).
108 To identify the flavinylation site, we subjected the ARD bands in the PAGE gel (lanes *1* and
109 *3* in Fig. 2B) to in-gel trypsin digestion and MALDI-MS and MS/MS analysis. Based on ApbE
110 specificity (12), the flavinylation site was predicted in the ARD *FMN_bind* domain within the
111 tryptic peptide I_{436}PQQILDGQTLNIDVISGA**T**VSSQAVLDGVSNAVDLAGGNSEALR$_{480}$ (the
112 flavinylation motif is underlined, the acceptor residue shown in bold). This peptide should
113 demonstrate the monoisotopic MH^+ masses of 4944.5 in the flavinylated and 4506.3 in the non-
114 flavinylated states. The mass spectrum of the tryptic digestion of ARD produced in the ApbE-
115 lacking *E. coli* cells demonstrated only the presence of the non-flavinylated peptide (Fig. 3B),
116 whereas the flavinylated peptide predominated in the spectrum of ARD produced by the *ard-*
117 *apb*E coexpression (Fig. 3A). The MS/MS analysis of the peptide with the *m/z* of 4944.5 (Fig.
118 3B) revealed two main signals with *m/z* of 4488.3 and 4506.3 in the spectrum of fragmentation.
119 A likely corollary is that they resulted from FMN loss in the full (*m/z* = 456) or dehydrated (*m/z*
120 = 438) form (14). Other than *m/z* = 4944.5 candidates for flavinylated peptides were not
121 observed in the tryptic digest of ARD.
122 Our data indicate thus that ARD resembles *K. pneumoniae* cytoplasmic NADH:fumarate
123 oxidoreductase in that both proteins contain covalently bound FMN and non-covalently bound
124 FAD and FMN in a ratio 1:1:1. Based on these data, the spectra of ARD in the native state and
125 after denaturation with SDS (1%, 5-min incubation at 80°C), and the known extinction
126 coefficients for FAD and FMN in solution (15), the extinction coefficient for native ARD at 450
127 nm was estimated to be 39.5 $mM^{-1} cm^{-1}$. This estimation was based on the premise that
128 denaturation brings flavins into an aqueous environment.
129
130 **2. The enzymatic activities of ARD**
131 The substrate specificity of ARD was tested with a series of α,β-unsaturated carbonic acids,
132 listed in Table 2, as tentative electron acceptors from methyl viologen (MV). A negligible or
133 minimal activity was observed with most tested compounds, except for methacrylate and, in
134 particular, acrylate. The carboxyl group in the substrate is necessary, as no MV oxidation was
135 detected when acrylamide was used as an electron acceptor. The reactions with acrylate and
136 methacrylate were explored in some detail below.
137 The similarity of the domain structures of ARD and *K. pneumoniae* NADH:fumarate
138 oxidoreductase, in particular the presence of an *OYE-like* domain in both, raised the possibility
139 of NADH being the physiological electron donor for ARD (5). Indeed, NADH supported
140 acrylate and methacrylate reduction, as illustrated in Fig. 4 for acrylate. Acrylate was absolutely

141 required for NADH oxidation under anaerobic conditions and markedly accelerated the reaction
142 under aerobic conditions, wherein acrylate competed with oxygen as the alternative electron
143 acceptor. Importantly, acrylate did not support NADH oxidation by ARD deficient in covalently
144 bound flavin (Fig. 4, *upper trace*).

145 The NADH:acrylate oxidoreductase activity was pH-dependent, with a maximum between
146 pH 6.5 and 7.0 (see Supplementary Material). The apparent K_m value for NADH measured at pH
147 6.5 with 1 mM acrylate was 14 ± 1 μM. NADPH could not replace NADH as the electron donor.
148 Steady-state kinetic analysis was also performed at varied acrylate and methacrylate
149 concentrations using a fixed saturating NADH concentration (150 μM). This analysis yielded the
150 K_m values of 16 ± 1 for acrylate and 690 ± 140 μM for methacrylate. The respective k_{cat} values
151 for these substrates were 19 ± 1 and 2.5 ± 0.2 s^{-1}. Acrylate is thus a much "better" substrate for
152 ARD.

153 HPLC identified the sole product of acrylate reduction by ARD to be propionate (Fig. 5).
154 Thus, the ARD-catalyzed oxidoreductase reaction can be described as follows:

155 acrylate + NADH + H^+ → propionate + NAD^+.

156 ARD did not catalyze the reverse reaction of propionate oxidation with phenazine methosulfate
157 or dichlorophenolindophenol as the electron acceptor, resembling in this aspect all known
158 soluble fumarate reductases and related enzymes (2).

159

160 **3. Dependence of ARD biosynthesis in *V. harveyi* cells on growth conditions**

161 An RT-qPCR study indicated that the level of *ard* expression was quite low in the *V.*
162 *harveyi* cells grown aerobically in the absence of acrylate but increased ~100-fold in the
163 presence of 2 mM acrylate, the maximal concentration at which acrylate does not yet inhibit cell
164 growth significantly (Table 3). In contrast, the expression of *ard* was high without acrylate and
165 increased only twofold in its presence when the cells were grown under anaerobic conditions.
166 The maximal level of *ard* expression was higher under anaerobic conditions. The enzymatic
167 activity of ARD in cell lysates demonstrated similar trends (Table 3). These results indicated that
168 either oxygen absence or acrylate presence induces ARD biosynthesis. The effects of the two
169 factors are additive, and *ard* is maximally expressed under anaerobic conditions in the presence
170 of acrylate.

171

172 **DISCUSSION**

173 *V. harveyi* ARD contains a Met residue instead of His in the position that determines
174 fumarate C1 carboxylate binding in fumarate reductases (Table 1) and was therefore expected to
175 have a different substrate specificity. The results reported above indicated that ARD and possibly

176 other similar enzymes possess a previously unknown acrylate reductase activity. This is the
177 principal activity of ARD, which converts alternative substrates at much lower rates (Table 2).
178 The bulky methionine residue in the binding site of ARD appears to be the critical factor that
179 determines ARD specificity. Only fumarate and its analogs with smaller substituents in the left
180 part are converted at measurable rates, whereas those with more bulky substituents are not
181 converted. Methacrylate is a better alternative substrate than crotonate (Table 2), indicating that
182 the α-position in acrylate is more tolerable to substitutions than the β-position. The significant
183 activity against the bulkier fumarate may be explained by the conservation in ARD of the
184 threonine residue (Thr808) found, together with histidine, in Motif II of fumarate reductases
185 (Table 1).

186 Although ARD can reduce methacrylate, its catalytic efficiency (k_{cat}/K_m) with this substrate
187 is smaller by a factor of 330 compared to acrylate. Oppositely, known methacrylate reductases
188 do not reduce acrylate (16) or reduce it at much lower rates than methacrylate (8, 9). The two
189 enzymes also differ markedly in the active site motifs (Table 1).

190 Acrylate was a potent inducer of gene *ard* transcription, under aerobic conditions in
191 particular (Table 3), providing independent support to the notion that acrylate reductase is the
192 principal activity of ARD. On the other hand, these data shed light on the possible physiological
193 role of ARD in *V. harveyi* cells. The ability of acrylate to markedly induce ARD production
194 under both aerobic and anaerobic conditions suggests a role for ARD in acrylate detoxification.
195 Acrylate toxicity results from its being a potent electrophile capable of reacting with many
196 cellular components (17, 18). A known way of acrylate detoxification involves NADPH-
197 dependent reduction of acryloyl-CoA by the protein AcuI to yield propionyl-CoA (18).
198 However, acryloyl-CoA is much more toxic than acrylate (18), making ARD-catalyzed acrylate
199 removal before its conversion to acryloyl-CoA a more efficient way of detoxification. In these
200 circumstances, the role of AcuI may be auxiliary and consist in neutralizing acryloyl-CoA
201 formed from acrylate in competing reactions before its conversion by ARD. The proposed role of
202 ARD in acrylate detoxification is consistent with the gene *ard* localization in close vicinity to the
203 gene for another detoxicating enzyme, glutathione S-transferase (AIV07248 in *V. harveyi*), on
204 chromosome 2 in most *ard*-containing *Vibrio* species.

205 The high level of *ard* expression under anaerobic conditions even in the absence of acrylate
206 (Table 3) suggests that ARD may use acrylate as the terminal electron acceptor for NADH
207 regeneration at oxygen deficiency. The ability of *Halodesulfovibrio aestuarii* (formerly known
208 as *Desulfovibrio acrylicus*) to use acrylate as terminal electron acceptor has also been
209 documented, although the enzyme(s) responsible for the acrylate reduction has(ve) not been
210 identified (19). Moreover, *V. harveyi* cells can use acrylate as the only carbon and energy source

211 (20). This makes acrylate detoxification in *V. harveyi* an energy-saving process—instead of
212 consuming energy, like in the detoxification pathways involving glutathione S-transferase, the
213 ARD-catalyzed reaction produces propionate, a "fuel" under aerobic conditions. Also of
214 importance, acrylate reduction helps deplete cells of NADH, which is crucial under anaerobic
215 conditions. The interplay between ARD's detoxification and energy production functions is
216 determined by oxygen availability. As *ard* expression is induced by acrylate under both aerobic
217 and anaerobic conditions, detoxification seems to be the primary function. If NADH reoxidation
218 were the primary function of ARD, the induction would have been only observed in the absence
219 of oxygen, like with other enzymes, such as NADH:fumarate oxidoreductase (5) and urocanate
220 reductase (10). Further, if the primary function were propionate accumulation, ARD production
221 would be stimulated by acrylate only under aerobic conditions because propionate is not
222 fermentable.

223 The exogenous nature of acrylate in *V. harveyi* is supported by the findings that this
224 bacterium is a common inhabitant of acrylate-rich niches, for instance, coral mucus (20). Marine
225 bacteria of the *Vibrio* genus demonstrate a positive taxis test with acrylate (21). What is the
226 source of acrylate in the environment? The primary precursor of acrylate in the living world is
227 dimethylsulfoniopropionate (DMSP) (22), which is produced and accumulated in high
228 concentrations in many marine algae as a compatible solute. DMSP conversion into acrylate is
229 catalyzed by the DMSP lyases DddL, DddP, DddQ, DddW, and DddY (22), explaining the
230 abundance of acrylate in many marine ecological niches and the presence of ARD homologs in
231 the *Vibrio* bacteria, which often inhabit these niches. Noteworthy, genes for the DMSP lyases are
232 absent in the *V. harveyi* genome, and *V. harveyi* cells do not convert DMSP or use it as a sole
233 carbon source (data not shown), which is consistent with the exogenous nature of acrylate in
234 them.

235 Acrylate reductase activity appears to be also indispensable in many terrestrial niches,
236 including human symbionts and pathogens. Genes for ARD-like proteins are found in the
237 genomes of certain non-marine bacteria, such as *Staphylococcus pasteuri* and *S. warneri* (human
238 pathogens); *S. lugdunensis*, *S. massiliensis*, and *S. epidermidis* (humane skin microbiome);
239 *Dickeya zeae* and *Paenibacillus brasilensis* (plant pathogens and symbionts); *Gilliamella apicola*
240 (bee intestine symbiont). The occurrence of ARD-containing bacteria in human pathogens may
241 make ARD an important drug target. Disturbances in the gut microbiome may cause the
242 accumulation of the toxic products of fermentation and anaerobic respiration, leading to various
243 diseases (23). The case of urocanate respiration is relevant and illustrative in this respect.
244 Molinaro *et al*. (24) demonstrated an association of urocanate respiration with type 2 diabetes,
245 and Koh *et al.* (25) further determined that imidazolylpropionate, the product of urocanate

246 reduction, causes glucose intolerance by inhibiting mTORC1 and, hence, suppressing insulin
247 signal transduction. These findings, which opened new perspectives in type 2 diabetes treatment,
248 emphasize the importance of identifying alternative anaerobic respiration types in microbes.
249
250
251
252
253 **MATERIALS AND METHODS**
254 *Production and isolation of ARD*
255 An expression vector for the C-terminal 6×His-tagged ARD protein was constructed by
256 amplifying the *ard* gene (GenBank Gene ID: 57822953) by PCR with a high fidelity Tersus PCR
257 kit (Evrogen) and the primer pair 5'-GAGGAATAAATTTATGGCTCAGTTAGTCGAT / 5'-
258 GGAAACAAGATCAGATGCACTCTC using the genomic DNA of *V. harveyi* as the template.
259 The resulting 3028-bp fragment was cloned into the pBAD-TOPO vector (Invitrogen), yielding
260 the pBAD_VHRD plasmid. The 6×His-tagged ARD protein was produced in *Escherichia coli*
261 BW25113 or /pΔhis3 cells and purified using metal chelate chromatography as described
262 previously (7).
263 *Analysis of flavin groups*
264 The relative amounts of covalently and non-covalently bound flavins in the recombinant ARD
265 were determined by HPLC and spectral analyses of the denatured protein as described by
266 Barquera *et al.* (26). Non-covalently bound flavins were separated by HPLC as described
267 elsewhere (7). SDS-PAGE was performed using 10% (w/v) polyacrylamide gels (27). The gels
268 were stained with PageBlue™ protein staining solution (Fermentas). Covalently bound flavins
269 were detected by scanning unstained gels with a Typhoon™ FLA 9500 laser scanner (GE
270 Healthcare) with excitation at 473 nm and the detection of emission using the SYBR Green II
271 protocol according to the manufacturer's recommendations. The in-gel trypsin digestion of ARD
272 and MALDI-MS and MS/MS analysis were done as described previously (14).
273 *Enzymatic activities*
274 NADH- and MV-supported activities of ARD were determined spectrophotometrically by
275 following the oxidation of NADH or MV (5). The assay medium contained 1 mM MV, 1 mM
276 electron acceptor, and 100 mM Tris-HCl (pH 8.0) or 150 μM NADH, 1 mM electron acceptor,
277 10 mM glucose, 5 U/mL glucose oxidase, 5 U/mL catalase, and 100 mM Mes-KOH (pH 6.5).
278 MV was pre-reduced with sodium dithionite until the absorbance at 606 nm of approximately 1.5
279 was obtained. The NADH-supported reaction was also measured under aerobic conditions

280 without glucose oxidase and catalase. One unit of enzyme activity was defined as the amount of
281 the enzyme that catalyzes the oxidation of 1 μmol NADH or 2 μmol MV per 1 min.
282 The pH-dependence of NADH:acrylate oxidoreductase activity was measured in a 100 mM
283 BIS-TRIS propane-citrate buffer, pH 4.5–9.0, containing 5 U/mL glucose oxidase, 5 U/mL
284 catalase, 10 mM glucose, 150 μM NADH, and 1 mM potassium acrylate.
285 In the experiments aimed at identification of the product of acrylate reduction, the reaction
286 medium contained 5 mM acrylate, 20 mM sodium dithionite, 50 μM MV, and 100 mM Tris-HCl
287 (pH 8.0). The reaction was performed in a 3.2-mL sealed cuvette completely filled with the
288 reaction mixture. Acrylate reduction was initiated by adding 0.5 μM ARD and terminated after
289 60 min by adding 5% (vol./vol.) $HClO_4$. In the control experiment, $HClO_4$ was added before
290 ARD. Precipitated protein was removed by centrifugation, and carbonic acids were isolated from
291 the samples by double extraction with diethyl ether (2 × 1.5 mL). The ether was evaporated
292 under a stream of air, and the residue was dissolved in 1 mL of aqueous 0.05% H_3PO_4. The
293 samples thus prepared were separated by HPLC on a ProntoSil-120-5-C18 AQ column using a
294 Milichrom A-02 chromatograph (both from Econova, Novosibirsk, Russia). The column was
295 pre-equilibrated with aqueous 0.05% H_3PO_4 solution and eluted with a linear gradient of 0% to
296 10% aqueous methanol containing 0.05% H_3PO_4 at a flow rate of 0.2 mL/min with UV detection
297 at 220 nm.
298 Propionate dehydrogenase activity was assayed by measuring the reduction of 2,6-
299 dichlorophenolindophenol (DCPIP) at 600 nm. The assay mixture contained 2 mM Tris-
300 propionate, 2 mM phenazine methosulphate, 25 μM DCPIP, and 100 mM Mes-KOH, pH 6.5.
301 *Cultivation of V. harveyi cells*
302 *V. harveyi* cells were grown aerobically or anaerobically at 32°C up to the middle of
303 exponential phase in a mineral medium containing 20 g/L NaCl, 0.7 g/L KCl, 1 g/L
304 $MgSO_4 \times 7(H_2O)$, 0.5 g/L NH_4Cl, 0.5 mM Na_2HPO_4, 2 g/L sucrose, 0.5 g/L yeast extract, 50 mM
305 Tris-HCl (pH 8.0). When required, the medium was supplemented with 2 mM potassium
306 acrylate. Cleared cell lysate was prepared as described (28) and assayed for MV:acrylate
307 oxidoreductase activity. Protein concentration was determined by the bicinchoninic acid method
308 (29) using bovine serum albumin as the standard.
309 *Quantitative reverse transcription polymerase chain reaction (RT-qPCR)*
310 RNA extraction from *V. harveyi* cells and cDNA synthesis were performed as described
311 (30). RT-qPCR assays were done with the qPCRmix-HS SYBR kit (Evrogen), using the cDNA
312 preparations as templates and 5'-CGGCGCAAACACATACCT / 5'-
313 GCCCGGTTGTTCAATCTCT as primer pair. 16S rRNA was used for data normalization
314 (primer pair 5'- CAGCCACACTGGAACTGAGA / 5'- GTTAGCCGGTGCTTCTTC). Serial

315 dilutions of *V. harveyi* genomic DNA, wherein the genes for ARD and 16S rRNA are present in
316 a 1:12 ratio (31), were used for calibration.
317
318 **Acknowledgements**
319 This work was supported by the Russian Science Foundation (project # 22-24-00133). MALDI
320 MS and laser scanner facilities became available to us in the framework of the Moscow State
321 University Development Program PNG 5.13.
322
323 **References**
324 1. Cecchini G, Schröder I, Gunsalus RP, Maklashina E. 2002. Succinate dehydrogenase and
325 fumarate reductase from *Escherichia coli*. Biochim Biophys Acta 1553:140–157.
326 2. Leys D, Tsapin AS, Nealson KH, Meyer TE, Cusanovich MA, Van Beeumen JJ. 1999.
327 Structure and mechanism of the flavocytochrome *c* fumarate reductase of *Shewanella*
328 *putrefaciens* MR-1. Nat Struct Biol 6:1113–1117.
329 3. Reid GA, Miles CS, Moysey RK, Pankhurst KL, Chapman SK. 2000. Catalysis in fumarate
330 reductase. Biochim Biophys Acta 1459:310–315.
331 4. Besteiro S, Biran M, Biteau N, Coustou V, Baltz T, Canioni P, Bringaud F. 2002. Succinate
332 secreted by *Trypanosoma brucei* is produced by a novel and unique glycosomal enzyme,
333 NADH-dependent fumarate reductase. J Biol Chem 277:38001–38012.
334 5. Bertsova YV, Oleynikov IP, Bogachev AV. 2020. A new water-soluble bacterial NADH:
335 fumarate oxidoreductase. FEMS Microbiol Lett 367:fnaa175.
336 6. Kim S, Kim CM, Son YJ, Choi JY, Siegenthaler RK, Lee Y, Jang T-H, Song J, Kang H,
337 Kaiser CA, Park HH. 2018. Molecular basis of maintaining an oxidizing environment under
338 anaerobiosis by soluble fumarate reductase. Nat Commun 9:4867.
339 7. Bertsova YV, Kostyrko VA, Baykov AA, Bogachev AV. 2014. Localization-controlled
340 specificity of FAD:threonine flavin transferases in *Klebsiella pneumoniae* and its
341 implications for the mechanism of Na^+-translocating NADH:quinone oxidoreductase.
342 Biochim Biophys Acta 1837:1122–1129.
343 8. Mikoulinskaia O, Akimenko V, Galouchko A, Thauer RK, Hedderich R. 1999. Cytochrome *c*-
344 dependent methacrylate reductase from *Geobacter sulfurreducens* AM-1. Eur J Biochem
345 263:346–352.
346 9. Gross R, Simon J, Kröger A. 2001. Periplasmic methacrylate reductase activity in *Wolinella*
347 *succinogenes*. Arch Microbiol 176:310–313.

348 10. Bogachev AV, Bertsova YV, Bloch DA, Verkhovsky MI. 2012. Urocanate reductase:
349 identification of a novel anaerobic respiratory pathway in *Shewanella oneidensis* MR-1. Mol
350 Microbiol 86:1452–1463.
351 11. Kees ED, Pendleton AR, Paquete CM, Arriola MB, Kane AL, Kotloski NJ, Intile PJ,
352 Gralnick JA. 2019. Secreted flavin cofactors for anaerobic respiration of fumarate and
353 urocanate by *Shewanella oneidensis*: cost and role. Appl Environ Microbiol 85:e00852-19.
354 12. Bogachev AV, Baykov AA, Bertsova YV. 2018. Flavin transferase: the maturation factor of
355 flavin-containing oxidoreductases. Biochem Soc Trans 46:1161–1169.
356 13. Bertsova YV, Fadeeva MS, Kostyrko VA, Serebryakova MV, Baykov AA, Bogachev AV.
357 2013. Alternative pyrimidine biosynthesis protein ApbE is a flavin transferase catalyzing
358 covalent attachment of FMN to a threonine residue in bacterial flavoproteins. J Biol Chem
359 288:14276–14286.
360 14. Serebryakova MV, Bertsova YV, Sokolov SS, Kolesnikov AA, Baykov AA, Bogachev AV.
361 2018. Catalytically important flavin linked through a phosphoester bond in a eukaryotic
362 fumarate reductase. Biochimie 149:34–40.
363 15. Cerletti P. 1959. Properties of riboflavin phosphates. Anal Chim Acta 20:243–250.
364 16. Arkhipova OV, Biryukova EN, Abashina TN, Khokhlova GV, Ashin VV, Mikoulinskaia
365 GV. 2019. Methacrylate-reducing activity of anaerobic bacteria *Anaeromyxobacter*
366 *dehalogenans* and *Denitrovibrio acetiphilus*. Microbiology 88:137–145.
367 17. Sieburth JM. 1961. Antibiotic properties of acrylic acid, a factor in the gastrointestinal
368 antibiosis of polar marine animals. J Bacteriol 82:72–79.
369 18. Todd JD, Curson AR, Sullivan MJ, Kirkwood M, Johnston AW. 2012. The *Ruegeria*
370 *pomeroyi acu*I gene has a role in DMSP catabolism and resembles *yhd*H of *E. coli* and other
371 bacteria in conferring resistance to acrylate. PLoS One 7:e35947.
372 19. van der Maarel MJEC, van Bergeijk S, van Werkhoven AF, Laverman AM, Meijer WG,
373 Stam WT, Hansen TA. 1996. Cleavage of dimethylsulfoniopropionate and reduction of
374 acrylate by *Desulfovibrio acrylicus* sp. nov. Arch Microbiol 166:109−115.
375 20. Raina JB, Tapiolas D, Willis BL, Bourne DG. 2009. Coral-associated bacteria and their role
376 in the biogeochemical cycling of sulfur. Appl Environ Microbiol 75:3492–3501.
377 21. Sjoblad RD, Mitchell R. 1979. Chemotactic responses of *Vibrio alginolyticus* to algal
378 extracellular products. Can J Microbiol 25:964–967.
379 22. Curson AR, Todd JD, Sullivan MJ, Johnston AW. 2011. Catabolism of
380 dimethylsulphoniopropionate: microorganisms, enzymes and genes. Nat Rev Microbiol
381 9:849–859.

382 23. Koh A, Bäckhed F. 2020. From association to causality: the role of the gut microbiota and its
383 functional products on host metabolism. Mol Cell 78:584–596.
384 24. Molinaro A., Bel Lassen P., Henricsson M., Wu H, Adriouch S, Belda E, Chakaroun R,
385 Nielsen T, Bergh PO, Rouault C, André S, Marquet F, Andreelli F, Salem JE, Assmann K,
386 Bastard JP, Forslund S, Le Chatelier E, Falony G, Pons N, Prifti E, Quinquis B, Roume H,
387 Vieira-Silva S, Hansen TH, Pedersen HK, Lewinter C, Sønderskov NB; MetaCardis
388 Consortium, Køber L, Vestergaard H, Hansen T, Zucker JD, Galan P, Dumas ME, Raes J,
389 Oppert JM, Letunic I, Nielsen J, Bork P, Ehrlich SD, Stumvoll M, Pedersen O, Aron-
390 Wisnewsky J, Clément K, Bäckhed F. 2020. Imidazole propionate is increased in diabetes
391 and associated with dietary patterns and altered microbial ecology. Nat Commun 11:5881.
392 25. Koh A, Molinaro A, Ståhlman M, Khan MT, Schmidt C, Mannerås-Holm L, Wu H, Carreras
393 A, Jeong H, Olofsson LE, Bergh PO, Gerdes V, Hartstra A, de Brauw M, Perkins R,
394 Nieuwdorp M, Bergström G, Bäckhed F. 2018. Microbially produced imidazole propionate
395 impairs insulin signaling through mTORC1. Cell 175:947–961.
396 26. Barquera B, Zhou W, Morgan JE, Gennis RB. 2002. Riboflavin is a component of the Na^+-
397 pumping NADH-quinone oxidoreductase from *Vibrio cholerae*. Proc Natl Acad Sci USA
398 99:10322–10324.
399 27. Laemmli UK. 1970. Cleavage of structural proteins during the assembly of the head of
400 bacteriophage T4. Nature 227:680–685.
401 28. Bertsova YV, Serebryakova MV, Anashkin VA, Baykov AA, Bogachev AV. 2019.
402 Mutational analysis of the flavinylation and binding motifs in two protein targets of the
403 flavin transferase ApbE. FEMS Microbiol Lett 366:fnz252.
404 29. Smith PK, Krohn RI, Hermanson GT, Mallia AK, Gartner FH, Provenzano MD, Fujimoto
405 EK, Goeke NM, Olson BJ, Klenk DC. 1985. Measurement of protein using bicinchoninic
406 acid. Anal Biochem 150:76–85.
407 30. Bertsova YV, Kulik LV, Mamedov MD, Baykov AA, Bogachev AV. 2019. Flavodoxin with
408 an air-stable flavin semiquinone in a green sulfur bacterium. Photosynth Res 142:127–136.
409 31. Wang Z, Hervey WJ 4th, Kim S, Lin B, Vora GJ. 2015. Complete genome sequence of the
410 bioluminescent marine bacterium *Vibrio harveyi* ATCC 33843 (392 [MAV]). Genome
411 Announc 3:e01493-14.
412

413 **Table 1.** Enzymatic activities and conserved amino acid residues of *FAD_binding_2* domain-containing proteins

Protein source	GeneBank protein ID	Pfam domains	Substrate reduced	Partial alignment of the *FAD_binding_2* domains		
				Motif 1	Motif II	Motif III
S. frigidimarina	ABI73517	*FAD_binding_2* *Cytochrom_c3_2*	Fumarate	Arg402…His504…Arg544	His365…Thr377	Glu378…Arg381…Arg402
K. pneumoniae	BAH63234	*FAD_binding_2* *FMN_bind* *OYE-like*	Fumarate	Arg756…His859…Arg899	His719…Ser731	Glu732…Arg735…Arg756
Geobacter sulfurreducens	AJY71931	*FAD_binding_2* *Cytochrom_c3_2**	Methacrylate	Arg353…His461...Arg501	Tyr311...Val323	Glu324...Arg330...Arg353
Wolinella succinogenes	CAE09288	*FAD_binding_2* *Cytochrom_c3_2**	Methacrylate	Arg344...His454...Arg495	Gly301...Val313	Ala387...Arg390...Arg411
S. oneidensis MR-1	Q8CVD0	*FAD_binding_2* *FMN_bind*	Urocanate	Arg411...His520...Arg560	Tyr373...Ile386.. .	Ala387...Arg390...Arg411
V. harveyi	AIV07243	*FAD_binding_2* *FMN_bind* *OYE-like*	?	Arg834...His940...Arg980	Met796...Thr808	Gly809...Val812...Arg834

414 *This domain is present as an additional subunit. All other listed proteins are monomeric.

415

416 **Table 2.** The reductase activity of ARD against a series of α,β-unsaturated carbonic acids
417 measured with MV as the electron donor.

Substrate (acid)		Activity* (s^{-1})
Fumaric	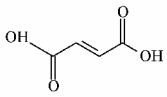	0.44 ± 0.08
Methacrylic		3.1 ± 0.4
Urocanic	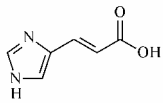	< 0.01
Acrylic		20 ± 3
Crotonic	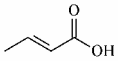	0.29 ± 0.05
Cinnamic	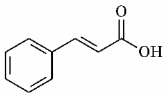	< 0.01

418

419 *The assay mixture contained 1 mM tentative substrate, ~100 μM of reduced MV, and 100 mM
420 Tris-HCl, pH 8.0.

421 **Table 3.** Correlation between *ard* transcription level and the acrylate reductase activity in the *V.*
422 *harveyi* cells cultivated in different conditions.

Growth conditions	*ard* mRNA/rRNA × 10^{-6}*	ARD activity (nmol·min^{-1}·mg^{-1})*
+O_2, no acrylate	0.094 ± 0.022	Not detected (<2)
+O_2, 2 mM acrylate	9.3 ± 0.8	18 ± 4
-O_2, no acrylate	7.5 ± 0.2	10 ± 4
-O_2, 2 mM acrylate	14.2 ± 1.1	38 ± 7

423 *From three independent experiments.

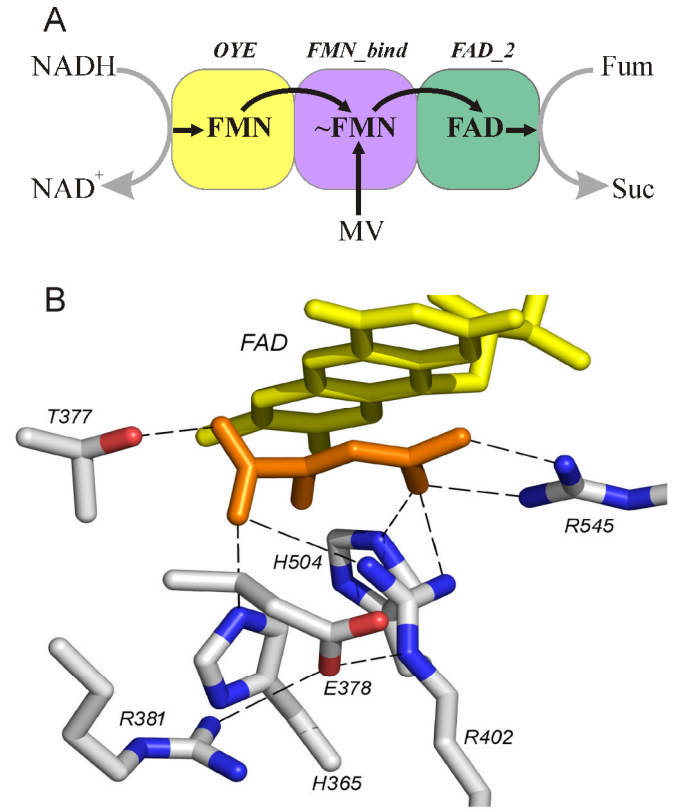

Fig. 1. The structural aspects of fumarate reductase. (A) The domain artichecture, prosthetic groups, and electron transport pathways from NADH/MV to fumarate in *K. pneumoniae* FRD. ~FMN denotes covalently bound FMN. (B) The structure of the substrate-binding site in the *FAD_binding_2* domain of *S. frigidimarina* Fcc_3 with bound malate molecule, shown in orange (PDB ID: 1QJD). Dashed lines show the polar contacts that fix the positions of malate carboxylates.

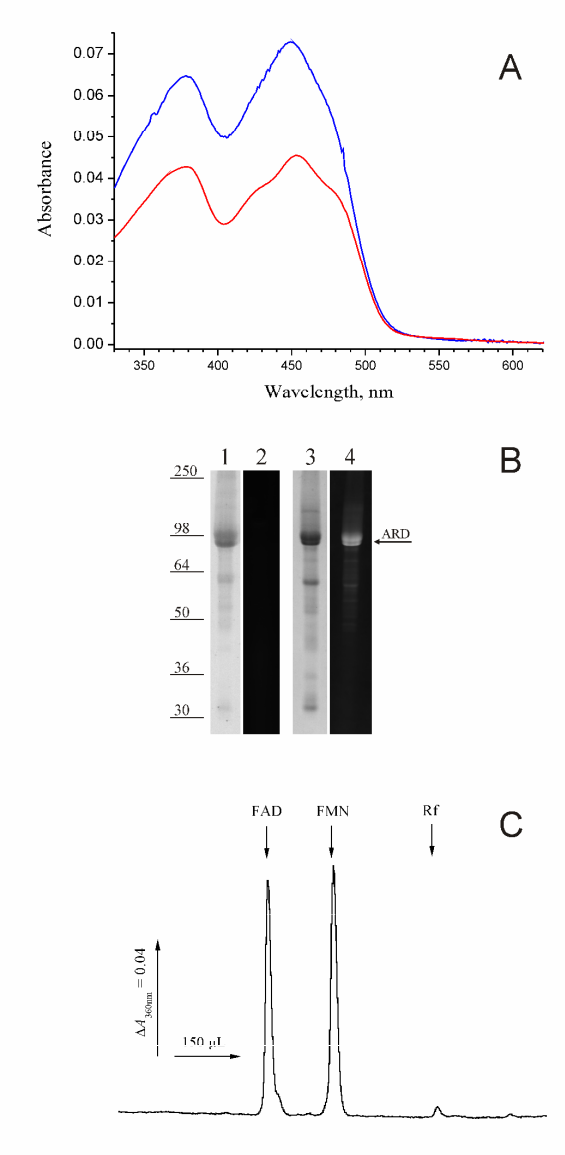

Fig. 2. Identification of the bound flavin groups. (A) Electronic absorption spectra of ARD preparations (1.8 µM) purified from ApbE-lacking (red curve) or ApbE-containing (blue curve) *E. coli* strain. Spectra were determined in 10 mM Tris-HCl buffer, pH 8.0, containing 100 mM KCl. (B) SDS-PAGE of ARD isolated from ApbE-lacking (lanes *1* and *2*) or ApbE-containing (lanes *3* and *4*) *E. coli* cells. The gels were stained with Coomassie Blue (lanes *1* and *3*) or photographed under illumination at 473 nm without staining (lanes *2* and *4*). The protein load was 4 µg per lane. The bars with numbers on the left side denote positions and molecular masses of marker proteins. (C) HPLC separation of non-covalently bound flavins of ARD. Retention times for authentic FAD, FMN, and riboflavin (Rf) are indicated by arrows.

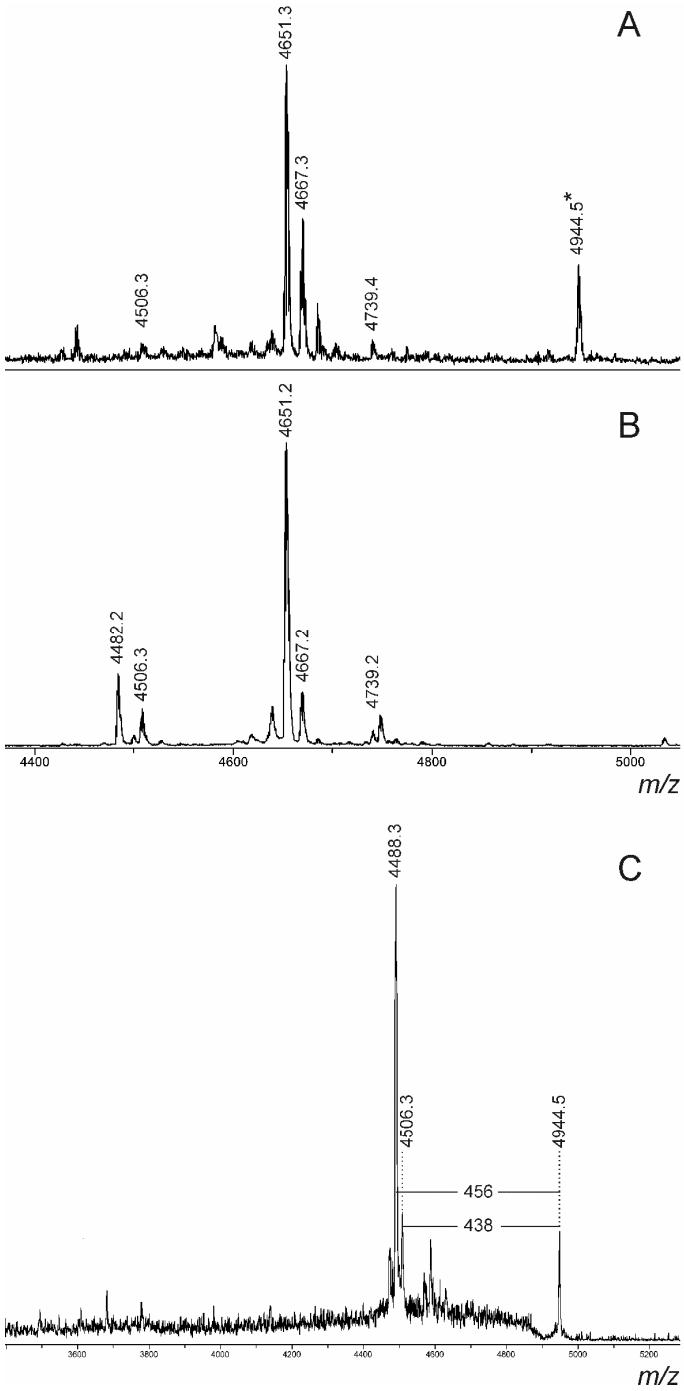

Fig. 3. Parts of the MALDI mass spectra of in-gel tryptic digests of ARD produced in ApbE-containing (A) or ApbE-lacking (B) *E. coli* strain. The asterisk on panel A marks the peak of the flavinylated peptide (*m/z* of 4944.5). (C) MS/MS spectrum of the peptide with *m/z* of 4944.5.

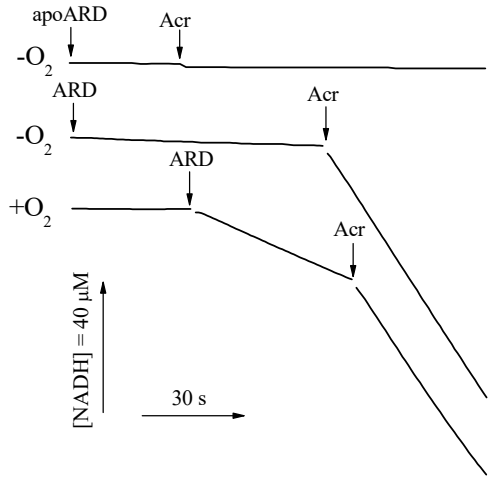

448

449 **Fig. 4.** Typical traces of NADH oxidation by ARD under anaerobic ($-O_2$) or aerobic ($+O_2$)
450 conditions. ARD isolated from the ApbE-lacking *E. coli* strain is designated as apoARD. Arrows
451 indicate additions of 30 nM ARD or apoARD and 1 mM acrylate (Acr). The assay mixture
452 contained 150 μM NADH and 100 mM Mes-KOH, pH 6.5. The anaerobic samples were also
453 supplemented with 10 mM glucose, 5 U/mL glucose oxidase, and 5 U/mL catalase.

454

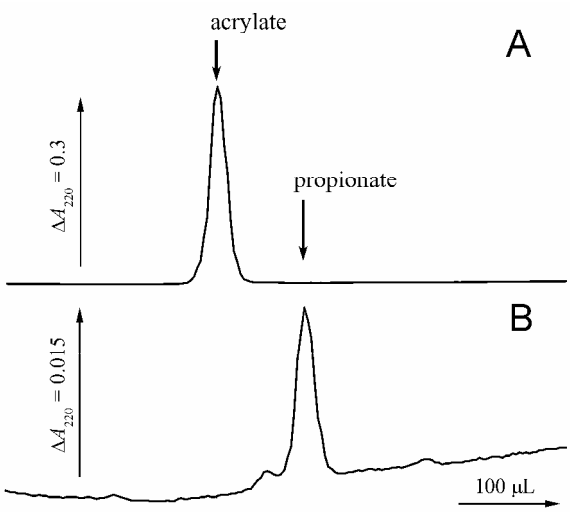

455

456 **Fig. 5.** HPLC identification of the product of acrylate reduction by ARD. Acrylate (5 mM) was
457 reacted with 20 mM sodium dithionite and 50 µM MV in the presence of 0.5 µM ARD. (A) The
458 extract of the reaction mixture before ARD addition. (B) The same after a 60-min incubation
459 with ARD. The elution volumes for authentic acrylic and propionic acids are indicated by
460 arrows, the corresponding retention times were 184 and 211 s. Of note, that extinction
461 coefficients for acrylate and propionate at 220 nm differed 20-fold.